

ON-ORBIT SPATIAL RESOLUTION ESTIMATION OF CBERS-1 CCD IMAGING SYSTEM FROM BRIDGE IMAGES

K. Bensebaa, G. J. F. Banon, L. M. G. Fonseca

Image Processing Division - National Institute for Space Research (INPE)
Av. dos Astronautas, 1758, 12201-027 São José dos Campos, Brazil
{camel, banon, Leila}@dpi.inpe.br

Commission WG I/2

KEY WORDS: CCD Camera, Spatial Resolution, Estimation, Modelling, Simulation, Measurements, Targets.

ABSTRACT:

The first China-Brazil Earth Resources Satellite (CBERS) was launched in 1999 and recently was substituted by CBERS-2. CBERS-1 and CBERS-2 have the same specifications and carry three sensors which combine features that are specially designed to cover the broad range of space and time scales involved in the monitoring and preservation of the ecosystem: Wide Field Imager (WFI), High Resolution CCD Camera (CCD) and Infrared Multispectral Scanner (IRMSS). In general, the imaging systems cause a blurring due to the cumulative effects of the instrumental optics (diffraction, aberrations, focusing error) and image motion induced by the movement of the satellite during imaging. This blurring can be understood by describing the imaging system in terms of the Point Spread Function (PSF). For a satellite sensor, the knowledge of the point spread function is of fundamental importance since it enables an objective assessment of spatial resolution through the parameter known as EIFOV (Effective Instantaneous Field of View). This paper describes an original approach to estimate the spatial resolution of the CBERS-1 CCD camera. The imaging system point spread function is modeled as a separable gaussian function. The PSF is estimated using images of Rio-Niteroi Bridge in Rio de Janeiro (Brazil) and the Lake Pontchartrain Causeway in Louisiana (United States). The results showed that the spatial resolution in across-track direction is outside the specifications for all bands while the spatial resolution in along-track direction is within the specification for all bands, except the band 4.

1. INTRODUCTION

The CBERS (China-Brazil Earth Resources Satellite) cooperative program has been jointly developed by China and Brazil for the building up a set of remote sensing satellites. CBERS-1 and CBERS-2 satellites were launched on October 14, 1999 and October 21, 2003, respectively. CBERS-1 carries onboard sensors, which combine features that are specially designed to cover the broad range of space and time scales involved in the monitoring and preservation of the ecosystem. During image acquisition, the imaging systems cause a blurring due to the cumulative effects of the instrumental optics (diffraction, aberrations, focusing error) and image motion induced by the movement of the satellite (Leger et al. 2002). This blurring effect can be modelled by the Point Spread Function (PSF) or by the Modulation Transfer Function (MTF) in the frequency domain.

The PSF and the MTF are of great importance in determining the spatial resolution of a system that is usually defined as its half-power response width (Bretschneider 2002). In general, the spatial response is estimated from the PSF in terms of the parameter known as EIFOV (Effective Instantaneous Field of View) (Slater, 1980). When the PSF is approximated by a gaussian function with standard deviation σ , the EIFOV is calculated as 2.66σ (Banon and Santos, 1993). Storey (2001) has provided a methodology to measure the Landsat-TM on-orbit spatial response using ground target such as bridges. Choi and Helder (2001) have used as targets airport runway and a tarp placed on the ground for on-orbit MTF measurement of IKONOS satellite sensor.

Before launching, band 4 (0,77 - 0,89 μm) of the CBERS-1 CCD camera presented a myopia distortion due to a problem in

the camera assembly. At this time, some image simulation tests were performed in order to check the possibility to improve its resolution spatial through restoration technique (Banon and Fonseca, 1998).

This paper describes an approach for the CBERS-1 CCD camera in-flight spatial resolution assessment. The CCD spatial response is modeled as a separable gaussian function in along-track and across-track directions of the satellite. On-orbit images of the Rio-Niteroi Bridge in Rio de Janeiro (Brazil) and the Lake Pontchartrain Causeway in Louisiana (United States) were used to estimate the spatial resolution in the along-track and across-track directions, respectively.

2. CBERS-1 OVERVIEW

CBERS-1 satellite carries on-board a multisensor payload with different spatial resolutions called: WFI (Wide Field Imager), IRMSS (Infrared MSS) and CCD (Charge Coupled Device) camera. The high-resolution CCD Camera has 4 spectral bands from visible light to near infrared and one panchromatic band (Table. 1). It acquires the earth ground scenes by pushbroom scanning, on 778 km sun-synchronous orbit and provides images of 113 km wide strips with sampling rate of 20 meters at nadir.

Spectral Bands	Number	Wavelength (μm)
Blue	B1	0,45 - 0,52
Green	B2	0,52 - 0,59
Red	B3	0,63 - 0,69
Near-Infrared	B4	0,77 - 0,89
Pan.	B5	0,51 - 0,73

Table 1. Spectral bands of the CCD sensor.

The signal acquisition system operates in two channels called CCD1 and CCD2. The first one generates images corresponding to B2, B3 and B4 while the second generates images corresponding to the bands B1, B3 and B5. In each channel (channel C1 and channel C2), three CCD chips per band were combined to generate about 6000 pixels per row.

3. PSF ESTIMATION METHODOLOGY

Basically, there exist three ways to determinate the PSF. The first one uses images with targets that must have well-defined shape and size as airport runway, bridges, etc or artificial target. The second method utilizes images acquired by higher resolution sensor, which are compared with the image under study. Finally, the third one uses the system design specifications and the system analytic model (Fonseca, 1987; Fonseca and Mascarenhas, 1987).

The first two approaches have the advantage of estimating the imaging system PSF by using in-flight images acquired by the system. In this work, the first approach was implemented and on-orbit images of bridges were chosen as target to estimate the spatial resolution in along-track and across-track directions.

3.1 Target Images

The Rio-Niteroi Bridge over Guanabara Bay (Figure 1 and Figure 2) was chosen as target to estimate the spatial resolution in the along-track direction. This bridge is 13.29-km long with only one deck and its width is 26.6 meters. On the other side, the Causeway Bridge over the Lake Pontchartrain

(Figure 3 and Figure 4) was used as target to estimate the spatial resolution in across-track direction. The bridge is constituted of two decks and a gap between them. The target is a 38.62-km long double deck bridge where each deck is 10.0 meters width and the gap is 24.4 meters width. The two decks of the bridge were constructed at different times (1956 and 1969) and exhibit slightly different reflectance. In addition, the water background is reasonably uniform.

3.2 Data preparation

The Rio-Niteroi Bridge and Lake Pontchartrain Causeway Bridge images were acquired by CBERS-1 CCD sensor on December 02, 2001 and October 06, 2002, respectively. Figure 5-top and Figure 6-left show, respectively, Rio-Niteoi bridge and Causeway bridge images of band 3. In order to facilitate the visualization, the images were enhanced by histogram contrast and zoomed up.

The images acquired by CBERS-1 system, before any kind of processing (raw data), present a striping effect as shown in the Figures 5 (top) and 6 (left). Odd columns are brighter than even columns. This is due to the non-uniform detector gains, since each detector is responsible for one column in the images. The processing procedure to remove the striping effect has been described in (Bensebaa, et al. 2003).

Figure 5 (bottom) and Figure 6 (right) display the processed images of Rio-Niteroi Bridge and Causeway Bridge, respectively. One can observe that the striping effect has been completely eliminated without removing the target information.

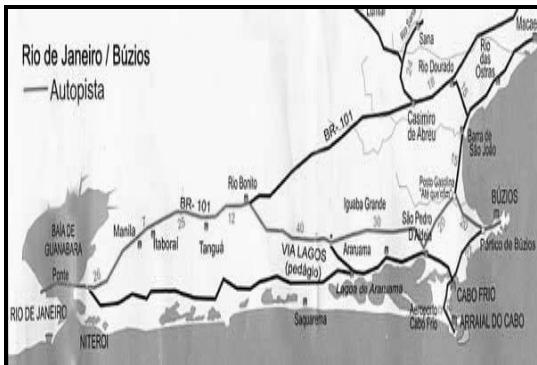


Fig.1 Map of Rio-Niteroi bridge in Guanabara bay.

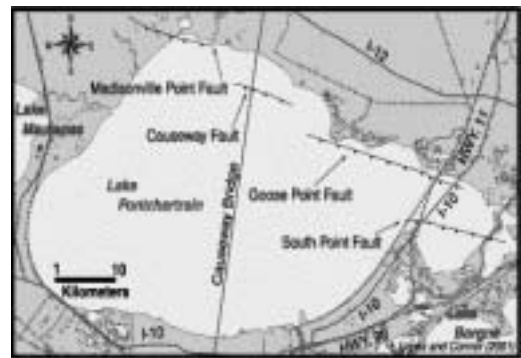


Fig.3 Map of Causeway bridge over Pontchartrain lake.



Fig.2 Aerial image of Rio-Niteroi bridge in Guanabara bay.



Fig.4 Aerial image of Causeway bridge over Pontchartrain lake.

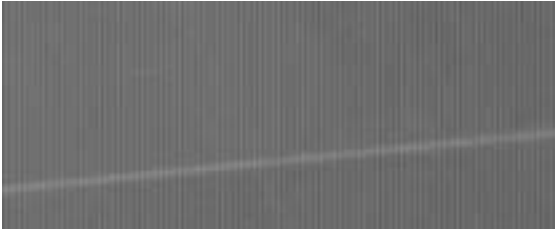


Fig.5 Rio-Niteroi bridge band3 (channel 1) image original and processed image.

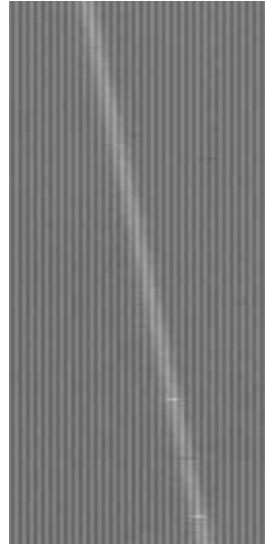


Fig.6 Causeway bridge band 3 (channel 1) image original and processed image.

3.3 Bridge model

3.3.1 Rio-Niteroi bridge model

Let \mathbf{Z} be the set of integer numbers. Let F_1 be a finite interval of \mathbf{Z} with an odd number of elements representing a vertical line of the digital scene domain in which the distance between two consecutive elements is one meter for convenience.

Let u_1 be the “center” point of F_1 . Based on radiometric and geometric features of the bridge over the Guanabara bay, the bridge model is the function f_1 on F_1 given by

$$f_1(x) = \begin{cases} t & \text{if } x \in [u_1 - 13, u_1 + 13] \\ s & \text{otherwise} \end{cases} \quad x \in F_1$$

where s, t are, respectively, the background (water body) and the deck radiometry.

3.3.2 Causeway bridge model

Let F_2 be a finite interval of \mathbf{Z} with an even number of elements representing an horizontal line of the digital scene domain in which the distance between two consecutive elements is one meter for convenience.

Let u_2 be the center point of F_2 . Based on radiometric and geometric features of the bridge over the Pontchartrain Lake, the bridge is modeled as the function f_2 on F_2 given by

$$f_2(x) = \begin{cases} t_1 & \text{if } x \in [u_2 - 22, u_2 - 13] \\ t_2 & \text{if } x \in [u_2 + 13, u_2 + 22] \\ s & \text{otherwise} \end{cases} \quad x \in F_2$$

where s, t_1, t_2 are the background, first deck and second deck radiometry information, respectively.

3.4 Bridge axis identification

According to Figure 5 and Figure 6, the bridge axis is a straight line. Consequently, it can be represented by a linear model.

Let the bridge image g be a mapping from $G = \mathbf{m} \times \mathbf{n}$, its domain, to K , its *gray-scale*, where $\mathbf{m} = [1, m] \subset \mathbf{Z}$ and $\mathbf{n} = [1,$

$n] \subset \mathbf{Z}$, where m and n are the number of rows and columns of the image g , respectively.

3.4.1 Rio-Niteroi bridge axis identification

Let c_1 be the mapping from \mathbf{n} to \mathbf{m} such that $c_1(j)$ ($j \in \mathbf{n}$) is the row number in \mathbf{m} , for which $g(c_1(j), j)$ is maximum in $\{g(i, j)\}_{i \in \mathbf{m}}$

Let $a, b \in \mathbf{R}$, such that

$$\sum_{i \in \mathbf{m}} ((a \cdot j + b) - c_1(j))^2 \text{ is minimum,}$$

then $a \cdot j + b$ ($j \in \mathbf{n}$) is the bridge center estimation along column j

3.4.2 Causeway bridge axis identification

Let c_2 be the mapping from \mathbf{m} to \mathbf{n} such that $c_2(i)$ ($i \in \mathbf{m}$) is the column number in \mathbf{n} , for which $g(i, c_2(i))$ is maximum in $\{g(i, j)\}_{j \in \mathbf{n}}$

Let $a, b \in \mathbf{R}$, such that

$$\sum_{i \in \mathbf{m}} ((a \cdot i + b) - c_2(i))^2 \text{ is minimum,}$$

then $a \cdot i + b$ ($i \in \mathbf{m}$) is the bridge center estimation along row i . In both cases (Rio-Niteroi and Causeway bridge axis identification), there are more measurements available than unknown parameters (a and b). Therefore, the QR-decomposition was used to generate a least square solution to an over-determined system of linear equations (Kreyszig, 1993).

3.5 System point spread function

The overall CBERS-1 CCD on-orbit PSF is a composition of the PSF of each sub-system PSF: optics, detector, electronics, etc. In this work the system point spread function is modeled as a 2D separable Gaussian function h_{σ_1, σ_2} on $F_1 \times F_2$ centered at (u_1, u_2) , that is,

$$h_{\sigma_1, \sigma_2}(x_1, x_2) = h_{\sigma_1}(x_1) \cdot h_{\sigma_2}(x_2)$$

where

$$h_{\sigma_1}(x_1) = \frac{1}{\sqrt{2\pi}\sigma_1} e^{-\frac{(x_1-u_1)^2}{2\sigma_1^2}} \quad x_1 \in F_1$$

and

$$h_{\sigma_2}(x_2) = \frac{1}{\sqrt{2\pi}\sigma_2} e^{-\frac{(x_2-u_2)^2}{2\sigma_2^2}} \quad x_2 \in F_2$$

3.6 Bridge image simulation

3.6.1 Rio-Niteroi bridge image simulation

The target image simulation of the Rio-Niteroi bridge uses the bridge center estimation of the Section 3.4 and a geometric transformation from real coordinate to discrete coordinate.

For a given column $j \in \mathbf{n}$, let $\hat{c}_1 = a \cdot j + b$:

Let G_1 , be a finite interval of \mathbf{Z} with an odd number of elements, denoted p ,

Let $v = (p + 1) / 2$ be the center of G_1 ,

Let assume that $G_1 + \left[\hat{c}_1 + \frac{1}{2} \right] - v \subset \mathbf{m}$,

Let T_{k_1} be a geometric transformation from G_1 to F_1 given by

$$T_{k_1}(y) = \left\lfloor 20 \cdot (y - v) + \frac{1}{2} \right\rfloor + u_1 + k_1 \quad y \in G_1$$

where

$$k_1 = \left\lfloor 20 \left(\left\lfloor \hat{c}_1 + \frac{1}{2} \right\rfloor - \hat{c}_1 \right) + \frac{1}{2} \right\rfloor$$

In the above definition, u_i is the center of the bridge, and k_1 represents how far the transformation of v is from u_i . Figure 7 shows the Rio-Niteroi Bridge model.

3.6.2 Causeway bridge image simulation

In this simulation, the method of Rio-Niteroi image simulation was used also to estimate the distance between the true bridge center and the estimated bridge center.

For a given row $i \in \mathbf{m}$, let $\hat{c}_2 = a \cdot i + b$

Let G_2 , be a finite interval of \mathbf{Z} with an even number of elements, denoted p .

Let assume that $G_2 + \left[\hat{c}_2 \right] - \frac{p}{2} \subset \mathbf{n}$.

Let T_{k_2} be a geometric transformation from G_2 to F_2 given by

$$T_{k_2}(y) = 20 \cdot (y - v) + u_2 + k_2 \quad y \in G_2,$$

where $v = (p + 1) / 2$ is the ‘‘center’’ of G_2 and

$$k_2 = \left\lfloor 20 \left(\frac{1}{2} + \left\lfloor \hat{c}_2 \right\rfloor - \hat{c}_2 \right) + \frac{1}{2} \right\rfloor$$

In the above definition u_2 is the center of the bridge, and k_2 represents how far the transformation of v is from u_2 .

In the Causeway bridge image simulation, the bridge center estimation \hat{c}_2 is actually biased due to the different radiometry of the two decks. Accordingly, k_2 is expressed as

$$k_2 = k_2' + \Delta$$

where

$$k_2' = \left\lfloor 20 \left(\frac{1}{2} + \left\lfloor \hat{c}_2 \right\rfloor - \hat{c}_2 \right) + \frac{1}{2} \right\rfloor$$

and Δ is a corrective term that takes into account the bridge center estimation bias. Since Δ assumes only a few integer values its estimation can be based on an exhaustive search. Figure 8 shows the Causeway Bridge model.

3.7 PSF estimation

Let g_1^j be the j^{th} target image column defined on G_1 given by

$$g_1^j(y) = g \left(\left\lfloor \hat{c}_1 + \frac{1}{2} \right\rfloor - v + y, j \right)$$

and let g_2^i be the i^{th} target image row defined on G_2 given by

$$g_2^i(y) = g \left(i, \left\lfloor \hat{c}_2 \right\rfloor - \frac{p}{2} + y \right).$$

The PSF estimation in the along-track direction consists of finding σ_1 such that g_1^j and $(f_1 * h_{\sigma_1}) \circ T_{k_1}$ best fits under the root mean square criteria. The PSF estimation in the across-track direction consists of finding σ_2 such that g_2^i and $(f_2 * h_{\sigma_2}) \circ T_{k_2}$ best fits under the root mean square criteria.

Let RMS_1 be the real number given by

$$\text{RMS}_1 = \left(\sum_{y \in G_1} \left((f_1 * h_{\sigma_1}) (T_{k_1}(y)) - g_1^j(y) \right)^2 \right)^{1/2}$$

The along-track estimation procedure is performed in two steps. Firstly, we look for t, s and σ_1 that minimize RMS_1 . Afterwards, using their mean values obtained from the first step, one looks for σ_1 that minimizes RMS_1 .

Let RMS_2 be the real number given by

$$\text{RMS}_2 = \left(\sum_{y \in G_2} \left((f_2 * h_{\sigma_2}) (T_{k_2}(y)) - g_2^i(y) \right)^2 \right)^{1/2}$$

The across-track estimation procedure is also performed in two steps. First of all, one looks for Δ, t_1, t_2, s and σ_2 that minimize RMS_2 . At the second step, using their mean values obtained from the first step, we look for σ_2 that minimizes RMS_2 . For both simulations (in the along-track and across-track-directions) the optimum values of σ_1 and σ_2 have been obtained by nonlinear programming (Himmelblau, 1972). Results of the best fitting between the image measurements and the simulated data, for band 3 in along-track and across-track directions, are shown in Figure 9 and Figure 10, respectively. Table 2 and Table 3 present the EIFOV values obtained by the method proposed in this work. EIFOV is related to the standard deviation σ so that $\text{EIFOV} = 2.66\sigma$ (Slater, 1980).

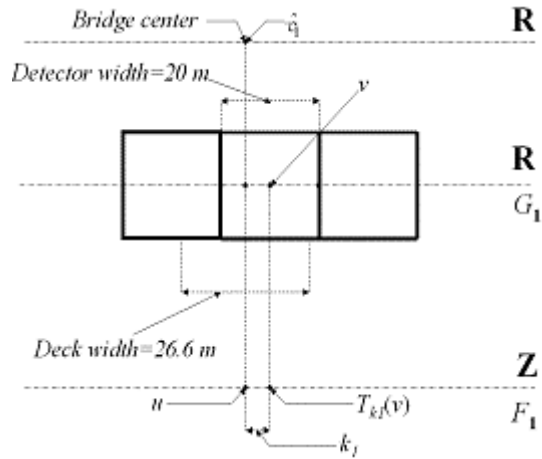


Fig.7 Rio-Niteroi bridge model.

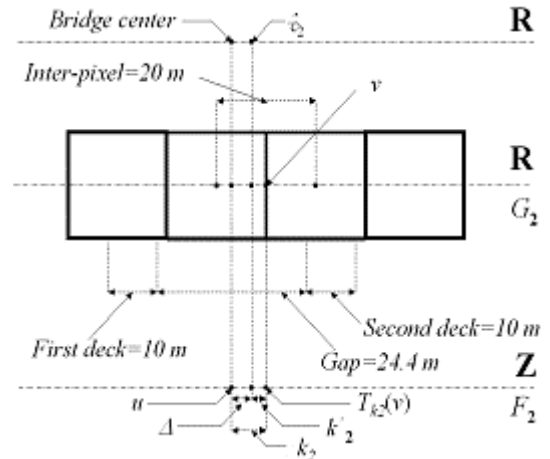


Fig.8 Causeway bridge model.

Bands	t	s	σ_1	EIFOV
B1	102.03	89.28	13.61	36
B2	62.8	54.29	13.92	37
B3/ C1	77.03	56.44	15.22	40
B3/C2	81.12	60.5	15.21	40
B4	80.12	61.72	24.22	64

Table 2: Estimated parameters in along-track direction.

Bands	t_1	t_2	s	Δ	σ_2	EIFOV
B1	69.44	73.5	47.67	-2,04	24.79	66
B2	69.92	72.79	47.65	-1.42	25.03	67
B3/ C1	103.4	113	58.32	-3.6	25	67
B3/C2	103.60	114.15	58.36	-3,78	25.24	67
B4	85.10	101.1	45.86	-4,59	30.52	81

Table 3: Estimated parameters in across-track direction.

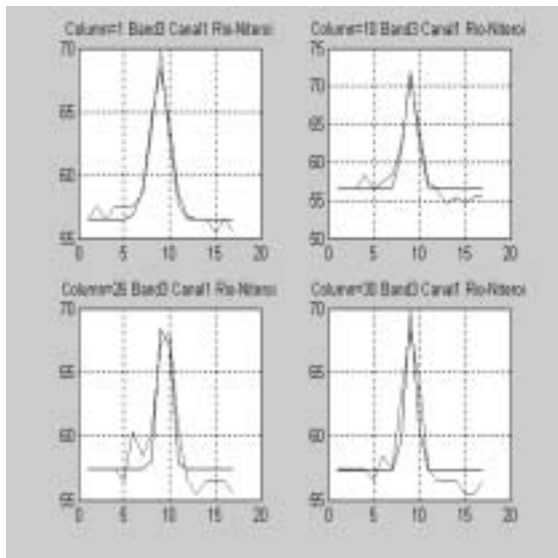


Figure 9. Along-track fitting for band 3.

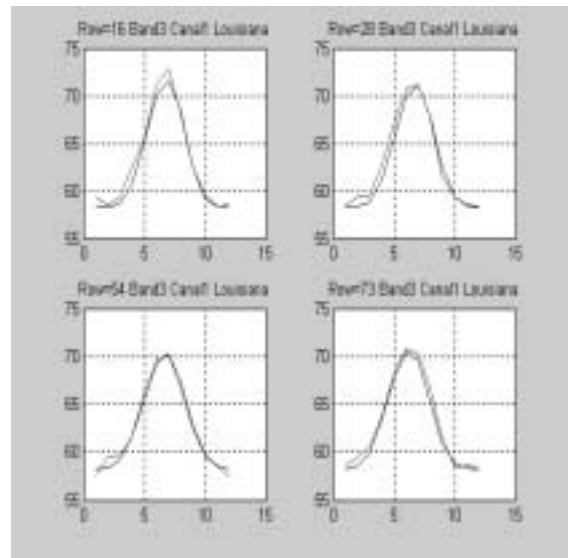


Figure 10. Across-track fitting for band 3.

4. CONCLUSION

An original approach for on-orbit spatial resolution assessment performance has been described. The method uses on-orbit data of the Pontchartrain Causeway Bridge in Louisiana and Rio-Niteroi Bridge in Rio de Janeiro. The main idea is to find the best fit between the image measurements and the simulated data. The results show that the spatial resolution in across-track direction does not conform to the specifications for any bands, while spatial resolution in the along-track directions meets the specifications for all bands except band 4. The low spatial resolution observed in across-track direction for bands 1, 2 and 3 was not observed on MTF measurements performed in laboratory. This degradation could be explained by the presence of mirror vibration when both sensors IRMSS and CCD work simultaneously. Besides this hypothesis, the observed degradation could be the result of an electronic joining between adjacent detectors. On the other hand, degradation verified for band 4 was expected due to problems in the CCD camera assembly.

5. REFERENCES

- Banon, G. J. F.; Santos, A. C. Digital filter design for sensor simulation: application to the Brazilian Remote Sensing Satellite. Sao Jose dos campos: INPE, 1993. 62 p. (INPE-5523-RPQ/665). Posted in the URLib digital library: <dpi.inpe.br/banon/1995/12.14.18.12>. Access in: 2003, Oct. 29.
- Banon, G. J. F.; Fonseca, L. M. G. CBERS simulation from SPOT and its restoration. CP 515, 12201-970 São José dos Campos, SP, Brazil: Instituto Nacional de Pesquisas Espaciais - INPE, 1998. Posted in the URLib digital library: <dpi.inpe.br/banon/1998/05.18.09.47>. Access in: 2003, Oct. 29.
- Bensebaa, K.; Banon, G. J. F.; Fonseca, L. M. G. On-orbit spatial resolution estimation of CBERS-1 CCD imaging system. In: III WorCAP, São José dos Campos - SP. 2003.
- Bretschneider, T. Blur identification in satellite imagery using image doublets. In: Asian Conference on Remote Sensing, 2002, Kathmandu, Nepal. *Proceedings...* 2002.
- Choi, T.; Helder, D. L. Techniques for measuring the in-orbit modulation transfer function (MTF) for high spatial resolution imaging satellite. In: High Spatial Resolution Commercial Imagery Workshop, Mar. 2001, Greenbelt, USA. *Proceedings...* 2001.
- Fonseca, L. M. G. Determinação e avaliação das funções de transferência de modulação (MTF) dos sistemas MSS e TM (Landsat-5). São Jose dos Campos: INPE, 1987. 19 p. (INPE-4187-RPE/543).
- Fonseca, L. M. G.; Mascarenhas, N. D. D. Determinação da função de transferência do sensor TM do satélite Landsat-5. In: Congresso Nacional de Matemática Aplicada e Computacional, 21-26 set. 1987, Gramado, BR. p. 297-302. (INPE-4213-PRE/1094)
- Himmelblau, D. M. *Applied Nonlinear Programming*. New York: McGraw-Hill Book Company, 1972.
- Kreyszig, E. *Advanced Engineering Mathematics*. John Wiley and Sons, Inc, 1993.
- Leger, D.; Viallefont-Robinet, F.; Meygret, A. In-flight refocusing and MTF assessment of SPOT5 HRG and HRS cameras, In: 9th International Symposium on Remote sensing, Aghia Pelagia (Greece), September 2002.
- Slater, P.N. *Remote Sensing Optics and Optical System*. London, Addison-wesley, 1980.
- Storey, J. C. Landsat 7 on-orbit modulation transfer function estimation. In: Sensors, Systems, and Next Generation Satellites V, 17-20 Sep. 2001, Toulouse, France. *Proceedings...* Bellingham, WA, USA: SPIE, 2001. p. 50-61. (*Proceedings of SPIE*, v.4540).